Extreme snowfall events linked to atmospheric rivers and surface air temperature via satellite measurements

Bin Guan,[1] Noah P. Molotch,[1,2] Duane E. Waliser,[1] Eric J. Fetzer,[1] and Paul J. Neiman[3]

Received 19 July 2010; revised 31 August 2010; accepted 14 September 2010; published 23 October 2010.

[1] Narrow bands of strong atmospheric water vapor transport, referred to as "atmospheric rivers" (ARs), are responsible for the majority of wintertime extreme precipitation events with important contributions to the seasonal water balance. We investigate relationships between snow water equivalent (SWE), precipitation, and surface air temperature (SAT) across the Sierra Nevada for 45 wintertime AR events. Analysis of assimilated and in situ data for water years 2004–2010 indicates that ARs on average generate ~4 times daily SWE accumulation of non-AR storms. In addition, AR events contributed ~30–40% of total seasonal SWE accumulation in most years, with the contribution dominated by just 1–2 extreme events in some cases. In situ and remotely sensed observations show that SWE changes associated with ARs are closely related to SAT. These results reveal the previously unexplored significance of ARs with regard to the snowpack and associated sensitivities of AR precipitation to SAT. **Citation:** Guan, B., N. P. Molotch, D. E. Waliser, E. J. Fetzer, and P. J. Neiman (2010), Extreme snowfall events linked to atmospheric rivers and surface air temperature via satellite measurements, *Geophys. Res. Lett.*, *37*, L20401, doi:10.1029/2010GL044696.

1. Introduction

[2] Along the West Coast of the United States, a significant proportion of wintertime precipitation is derived from infrequent intense storms associated with "atmospheric river" (AR) conditions. Strong water vapor fluxes in the lower atmosphere associated with ARs, when directed toward the mountain topography, are especially favorable for orographic precipitation. The hydrologic importance of ARs to the West Coast has been established with regard to precipitation [*Neiman et al.*, 2008a], stream flow and flooding [*Ralph et al.*, 2006; *Neiman et al.*, 2008b; *Leung and Qian*, 2009]. The importance of ARs with respect to snow accumulation has received less attention despite the dominance of the snowpack with regard to the cycling of water and energy, the functioning of ecosystems, and the availability of water for agriculture, hydropower, and municipal demands [*Bales et al.*, 2006]. In this regard, the seasonal snowpack of the Sierra Nevada is dominated by "leading" snowfall events (the biggest event of each season), representing a larger percentage of total seasonal snow accumulation (17%) than in the Pacific Northwest (12%) or interior regions (~11%) [*Serreze et al.*, 2001]. As the primary driver of intense moisture flux in the region, ARs therefore, may have regional impacts that dwarf less intense non-AR storms. Similarly, the sensitivity of AR dynamics to hydroclimatic conditions and change may dictate changes in water availability associated with climate change. Stronger ARs with a greater amount of total column water vapor are favored by warmer air temperatures. On the other hand, increases in surface air temperature may lead to a shift from snowfall to rainfall [*Stewart et al.*, 2004; *Serreze et al.*, 2001]. Model projections of air temperature indicate a potential change of up to 3–4°C in some West Coast regions for the end of the century [*Intergovernmental Panel on Climate Change*, 2007]. The implications of a potential shift from snowfall to rainfall for intense AR storms are significant with regard to terrestrial water cycling and reservoir demands whereby significant snowpack water storage is lost and significant increases in flood peaks and flood risk may result.

[3] The objectives of this research are twofold: (1) evaluate the relative contribution of ARs to total seasonal snow accumulation and (2) explore the possible effects of air temperature on AR rain-snow partitioning.

2. Data

2.1. Snow Water Equivalent (SWE) and Precipitation

[4] Due to the large spatial heterogeneity, domain averaged SWE in the Sierra Nevada, of interest here, cannot be accurately obtained from relatively sparse point observations [*Molotch and Bales*, 2005, 2006]. For this, daily SWE estimates from the 1-km resolution Snow Data Assimilation System (SNODAS) product are used. SNODAS assimilates ground, airborne and satellite snow observations [*Carroll et al.*, 2001]. Errors are estimated to be ~11% of the maximum SWE, on average, based on snowpit observations in Colorado during 2002–2003 [*Rutter et al.*, 2008]. Precipitation input to SNODAS is also used.

2.2. Surface Air Temperature (SAT) and Integrated Water Vapor (IWV)

[5] The Atmospheric Infrared Sounder (AIRS) version-5 level-3 standard temperature and water vapor retrievals (1° × 1° grid) are used. AIRS SATs are more certain over oceans (1 K error) relative to land (2–3 K error) [*Aumann et al.*, 2006; *Olsen et al.*, 2007]. We also examine ERA Interim reanalysis 2-meter air temperature (1.5° × 1.5° grid) [*Uppala et al.*, 2008].

[1]Jet Propulsion Laboratory, California Institute of Technology, Pasadena, California, USA.
[2]Department of Geography and Institute for Arctic and Alpine Research, University of Colorado at Boulder, Boulder, Colorado, USA.
[3]Physical Sciences Division, Earth System Research Laboratory, NOAA, Boulder, Colorado, USA.

0094-8276/10/2010GL044696

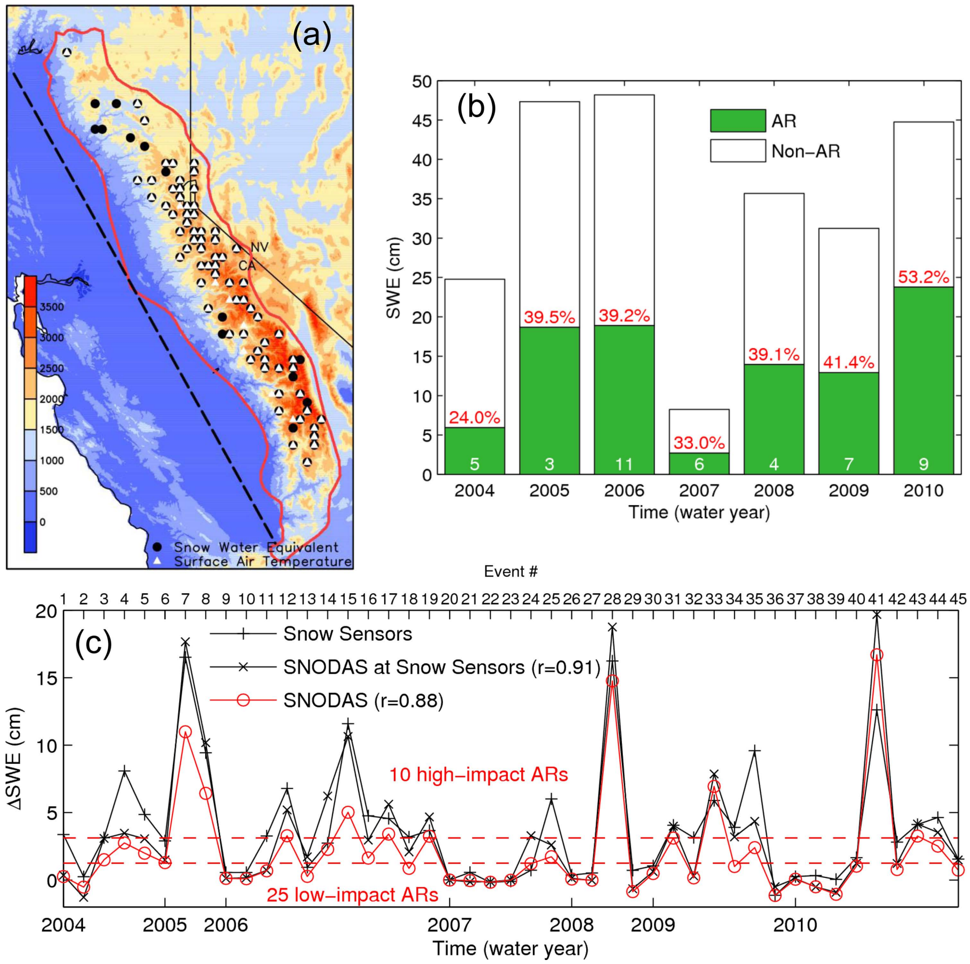

Figure 1. (a) Elevation (m; shading) map showing the Sierra Nevada domain (red contour) and the snow sensor network (dots). Those sensors equipped with surface air temperature readings are marked with triangles. (b) SNODAS estimates of SWE (cm) over the Sierra Nevada associated with atmospheric rivers (ARs) compared to the total seasonal (November–March) accumulation during WY2004–2010. Also shown is the number of AR events each year (white numerals) and their percentage contribution to the seasonal snow accumulation (red numerals). (c) ΔSWE (cm) associated with individual AR events during WY2004–2010 based on snow sensor observations (plus signs), SNODAS re-sampled at snow sensor locations (crosses), and SNODAS averaged over the Sierra Nevada domain above 1500 m (circles). Correlations between snow sensor and the two versions of SNODAS ΔSWE are shown in the legend. The dashed lines indicate 1/4 standard deviation above and below the mean SNODAS ΔSWE of the 45 events. ΔSWE is summed from one day before to one day after an AR event based on daily values.

2.3. Atmospheric Rivers (ARs)

[6] The classification scheme of *Neiman et al.* [2008a] is used to define AR "events". This scheme uses twice daily IWV in the atmosphere, as observed by the Special Sensor Microwave Imager/Sounder, and identifies calendar dates when IWV values exceed 2 cm over narrow bands that are longer than 2000 km and narrower than 1000 km and intersect the U.S./Canada West Coast between 32.5 and 52.5°N. Here, only ARs land-falling in California are considered, and an AR event is defined to be either a single day or a multi-day period that satisfies the above IWV criteria on each day. These events typically last for 1–2 days, and largely vary in IWV/temperature structures, and overland impacts. The time window used to calculate accumulated SWE changes (ΔSWE)/precipitation includes one day before and one day after each AR event to accommodate for possible time lead/lag between AR conditions and actual precipitation.

2.4. In Situ Data

[7] Daily SWE values are obtained from 100 snow sensor sites over the analysis period (water year (WY) 2004–2010) (Figure 1a). For SAT, a total of 92 sites are used for which daily average temperatures are available for the latest five water years (WY2006–2010). These SAT measurements are hereafter referred to as in situ SAT.

3. Impact of ARs on SWE

[8] We focus on ARs' impacts on SWE accumulation given the importance of spring-summer snowmelt to stream flow and water supplies in this region. For each winter (November–March), the contribution of ARs to total SWE accumulation is calculated as the summation of the accu-

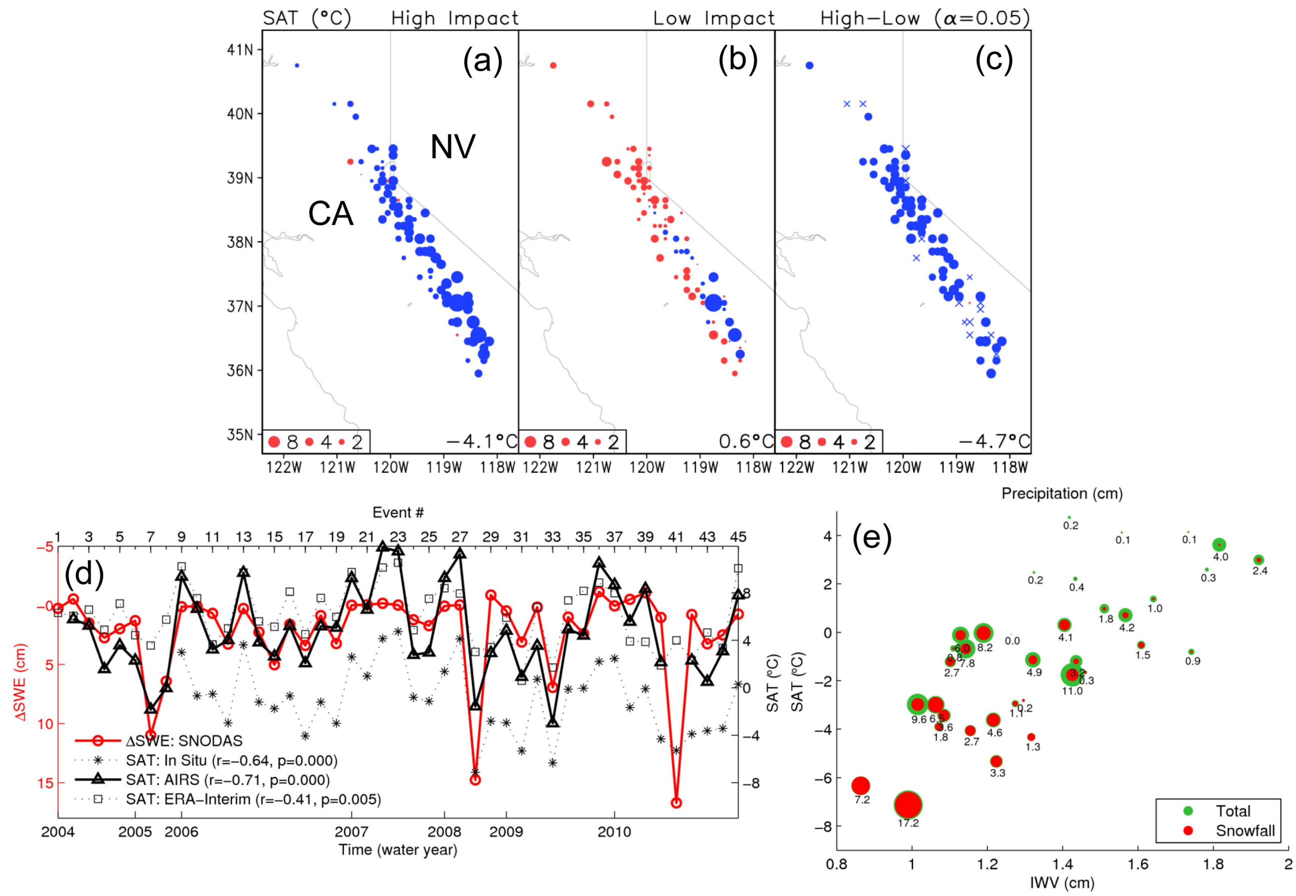

Figure 2. Daily mean surface air temperature (SAT; °C) composited over (a) high- and (b) low-impact ARs (i.e., those with ΔSWE 1/4 standard deviation above/below the mean; see Figure 1c). (c) Difference between Figures 2a and 2b, with statistically significant (insignificant) sites shown in dots (crosses) based on the Wilcoxon–Mann–Whitney test (α = 0.05). The size (area) of the dots/crosses is proportional to the magnitude of the temperature. Positive values are in red and negative values in blue. Spatial means are indicated in the lower-right corner of Figures 2a–2c. Data are from in situ observations at the snow sensor sites during WY2006–2010. (d) Sierra Nevada ΔSWE (cm) and SAT (°C) associated with individual AR events during WY2004–2010. SAT from three data sources are shown. Correlations (and *p*-values) between ΔSWE and SAT are indicated in the legend. The ΔSWE (SAT) values are areal averages above 1500 m (or over all available grid points for AIRS and ERA Interim), and are summed (averaged) from one day before to one day after an AR event based on daily values. Note that ΔSWE is shown on a flipped scale. (e) Precipitation (cm) associated with the AR events as a function of mean IWV (along the dashed line in Figure 1a) and SAT in the Sierra Nevada. Precipitation is from SNODAS. IWV and SAT are from AIRS retrievals and in situ measurements, respectively.

mulated ΔSWE over all AR events (Figure 1b). Non-AR contributions to total SWE are taken as the difference to the seasonal total accumulation. These calculations are based on the SNODAS assimilated SWE and are averaged over all 1 km pixels with elevation greater than 1500 m within the Sierra Nevada domain (Figure 1a, red contour). Note that the above elevation criteria are used in all subsequent calculations of domain averaged SWE. AR percentage contributions are relatively large (~40%) during the wetter water years of 2005, 2006 and 2008–2010. WY2006 had the highest frequency of ARs with 11 events (Figure 1c). Much fewer events (3 and 4, respectively) are observed during WY2005 and WY2008 but percentage contributions to the seasonal SWE are comparably high. The AR contribution to total SWE accumulation is dominated by just two events during WY2005 and a single event during WY2008 and WY2010 (Figure 1c). Several AR events occurred during the drier water years of 2004 and 2007, but with a higher percentage of SWE contributed by non-AR events.

[9] SWE accumulation associated with ARs varied significantly from year to year. For example, the amount in WY2006 (~19 cm) is about three times larger than WY2004 and about seven times larger than WY2007. On average, ARs generated ~4 times as much daily ΔSWE as non-AR storms (not shown).

[10] The time series of SNODAS ΔSWE over the 45 AR events during WY2004–2010 reveals large event-to-event variations in ΔSWE (Figure 1c, circles). The three largest AR events resulted in ΔSWE greater than 10 cm, whereas smaller events resulted in negligible changes in SWE. We define the "high-impact" ("low-impact") events as those with ΔSWE values 1/4 standard deviation above (below) the mean (Figure 1c, dashed lines). Four out of the 10 high-impact events are during the La Niña winter of 2005–06.

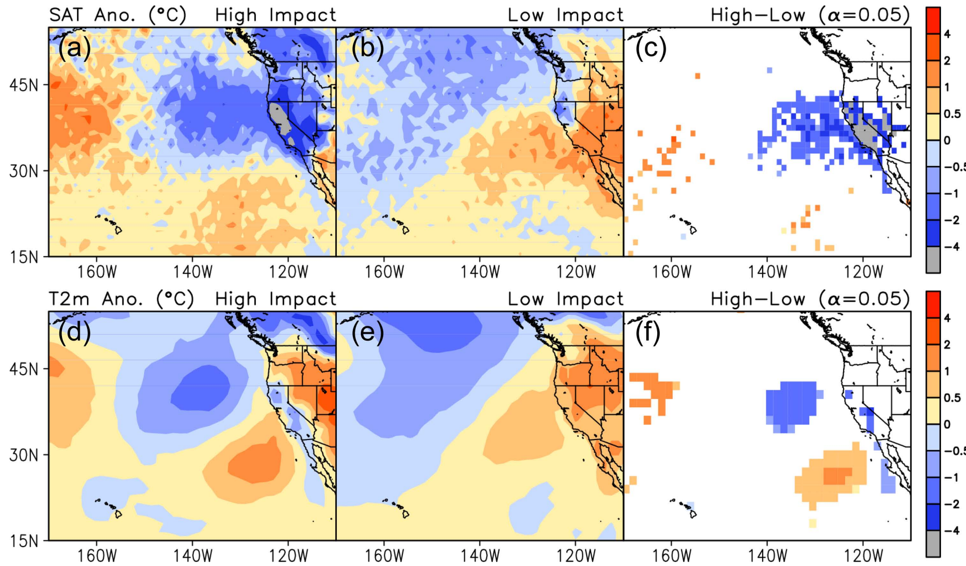

Figure 3. AIRS surface air temperature (SAT; °C) anomalies (relative to the daily climatology) composited over (a) high- and (b) low-impact ARs. (c) Difference between Figures 3a and 3b where statistically significant based on the Wilcoxon–Mann–Whitney test ($\alpha = 0.05$). (d–f) As Figures 3a–3c except with data from the ERA Interim reanalysis.

Interestingly, the two highest impact events in January 2008 (event #28, ΔSWE = 14.8 cm) and January 2010 (event #41, ΔSWE = 16.7 cm) occurred during a moderate-strong La Niña and El Niño, respectively.

[11] Comparisons of observed SWE at snow sensor locations and SNODAS SWE values re-sampled at snow sensor locations (Figure 1c, black lines) corroborate the domain-averaged SNODAS SWE results described above. Here the SNODAS re-sampled values reflect average SWE over the 1 km area surrounding snow sensor sites (i.e., points), which, due to the spatial heterogeneity in snow distribution, may not be representative of the point value [*Molotch and Bales*, 2005, 2006]. Because these point values are assimilated into the SNODAS estimates there is fairly good agreement between observed and SNODAS SWE at the snow sensor sites. As a result of this assimilation, SNODAS ΔSWE averaged across the Sierra Nevada domain (Figure 1c, circles) is well correlated with observed SWE (Figure 1c, plus signs). Relative to snow sensor observations, the SNODAS SWE estimates are more suitable for evaluating AR significance since the spatial variation in SWE is explicitly resolved and hence the domain average SWE is more adequately represented.

4. Connection Between ΔSWE and SAT

[12] High-impact versus low-impact AR events were associated with inter-storm differences in temperature (Figures 2a–2c). Average temperatures over the Sierra Nevada domain were −4.1°C and 0.6°C for high and low impact events, respectively. A linkage between SAT and ΔSWE is suggested during the AR events such that colder air temperatures are associated with increased snow accumulation.

[13] Time series of SNODAS ΔSWE averaged over the Sierra Nevada domain (as in Figure 1c) is shown in Figure 2d along with domain-average SAT from three data sources (in situ, AIRS, and ERA Interim). The in situ SAT is notably lower than AIRS and ERA Interim, partly due to the high-resolution spatial sampling of the complex terrain. Correlations (and p values) between the ΔSWE and SAT time series are indicated in the legend. Taking the in situ SAT as a reference ($r = -0.64$), AIRS is able to pick up the strong correlation of SAT to ΔSWE ($r = -0.71$), whereas the correlation based on ERA Interim SAT is considerably weaker although still statistically significant ($r = -0.41$). The negative correlations are indicative of the temperature controls on the rain-snow transition elevation and important local processes (e.g., orographically-induced adiabatic and diabatic cooling) during Sierra snowfall events, a detailed account of which is beyond the scope of this paper.

[14] SWE changes are greatly affected by the partitioning between snowfall and rainfall whereby decreases in SWE may result from rain-on-snow. The sensitivity of snow/rain ratio of AR precipitation to SAT is demonstrated in Figure 2e. Large snow/rain ratios occur when SAT is below freezing; total precipitation is meanwhile relatively large despite the smaller IWV content (note that SAT and IWV are correlated at 0.73). Based on Figure 2e, a warming of the land surface by a few °C, as in century-scale IPCC projections, could pose a potential challenge to regional water resources and management with reduced total precipitation and increased ratio of rain. The actual response in AR precipitation to warming temperatures would nonetheless depends on many factors, including the AR structure, date of occurrence, land-falling location, etc.

5. SAT Anomaly Patterns From AIRS and ERA Interim

[15] Both AIRS and ERA Interim data reveal similar SAT anomaly (raw minus daily climatology) patterns over the open ocean for both high impact (Figures 3a and 3d) and

low impact (Figures 3b and 3e) AR events. Specifically, a front structure is indicated by the strong temperature gradient offshore California, with cold anomalies to the north and warm anomalies to the south. The overall pattern is consistent with *Neiman et al.* [2008a] based on the NCEP–NCAR reanalysis 925-hPa air temperature.

[16] Notable differences between AIRS and ERA Interim SAT can be seen over the land surface. For AIRS, relatively large cold anomalies are seen in much of California associated with the high-impact AR events and relatively small warm/cold anomalies are seen during the low-impact AR events. The SAT contrast in the Sierra Nevada between the two types of events (Figure 3c) is in broad consistency with that suggested by Figure 2c. Compared to AIRS, ERA Interim shows much weaker cold anomalies during the high-impact AR events; the SAT contrast between the two types of events is also much smaller (Figure 3f).

[17] The improvement from AIRS over ERA Interim (as suggested by Figures 2d and 3) is likely due to its ability to sound lower into the middle tropospheric temperatures under partial cloud cover. The single assimilated radiosonde at Oakland may not properly constrain ERA Interim storm development over the Sierra Nevada. Global reanalyses (including ERA Interim) assimilate AIRS radiances, but use very stringent rejection criteria to avoid cloud contamination [*McNally et al.*, 2006]. This study suggests the AIRS SAT retrievals could lead to improved characterization of Sierra snowfall during AR events.

6. Conclusions

[18] AR percentage contributions to seasonal SWE accumulation are relatively large (~30–40%) during most years analyzed, with AR contribution dominated by just two events in WY2005 and a single event in WY2008 and WY2010. On average, ARs generate ~4 times as much daily ΔSWE as non-AR storms.

[19] In situ and remotely-sensed observations indicate that ΔSWE and SAT are closely related in the Sierra Nevada during AR events. Colder SAT was observed for high-impact ARs, whereas warmer SAT were observed for low-impact ARs; averaging to −4.1°C and 0.6°C, respectively. The strong negative correlation between observed ΔSWE and SAT ($r = -0.64$) is well captured by the AIRS satellite retrievals ($r = -0.71$), better from for the ERA Interim reanalysis (−0.41). Since AR storms are relatively warm (i.e., relatively close to the freezing/melting point), it is clear that partitioning of AR precipitation into snowfall versus rainfall is very sensitive to SAT with SAT differences comparable to the scale of warming in IPCC model projections of regional SAT changes for the end of the century. Detailed analyses of local and synoptic-scale atmospheric conditions are needed to improve predictions of future rain-snow partitioning during AR events. Atmospheric moisture/temperature profiles retrieved by AIRS, for example, provide new opportunities to explore the vertical structure of ARs. In addition, detailed observations and models of distributed snowpack processes [e.g., *Molotch*, 2009; *Molotch and Margulis*, 2008; *Durand et al.*, 2008] are needed to provide robust assessments of AR impacts. Next generation of both atmospheric and snow data assimilation products that include major improvements in the treatment of moisture and the global water cycle will also enable new insights into ARs' mechanisms and impacts.

[20] **Acknowledgments.** This research was supported by NSF EAR071160 and by NASA grant NNX08AH18G. B. Tian, M. Ralph, G. Wick, M. Dettinger, K. Weickmann and J. Kim are acknowledged for useful discussions and technical support. Data used in this study have been obtained online from NSIDC, CA DWR, NASA and ECMWF. DEW's and BG's contribution, and part of NPM's contribution, to this study was carried out on behalf of the Jet Propulsion Laboratory, California Institute of Technology, under a contract with the National Aeronautics and Space Administration.

References

Alpert, P. (1986), Mesoscale indexing of the distribution of the orographic precipitation over high mountains, *J. Clim. Appl. Meteorol.*, *25*, 532–545, doi:10.1175/1520-0450(1986)025<0532:MIOTDO>2.0.CO;2.

Aumann, H. H., S. Broberg, D. Elliot, S. Gaiser, and D. Gregorich (2006), Validation of the AIRS radiometric calibration for climate research using sea surface temperature measurements, *J. Geophys. Res.*, *111*, D16S90, doi:10.1029/2005JD006822.

Bales, R. C., N. P. Molotch, T. H. Painter, M. Dettinger, R. Rice, and J. Dozier (2006), Mountain hydrology of the western United States, *Water Resour. Res.*, *42*, W08432, doi:10.1029/2005WR004387.

Barros, A. P., and D. P. Lettenmaier (1994), Dynamic modeling of orographically induced precipitation, *Rev. Geophys.*, *32*, 265–284, doi:10.1029/94RG00625.

Carroll, T., D. Cline, G. Fall, A. Nilsson, L. Li, and A. Rost (2001), NOHRSC operations and the simulation of snow cover properties for the conterminous U.S., in *Proceedings of the 69th Annual Meeting of the Western Snow Conference*, pp. 1–14, Sun Valley, Idaho.

Durand, M., N. P. Molotch, and S. A. Margulis (2008), A Bayesian approach to snow water equivalent reconstruction, *J. Geophys. Res.*, *113*, D20117, doi:10.1029/2008JD009894.

Grubišić, V., R. K. Vellore, and A. W. Huggins (2005), Quantitative precipitation forecasting of wintertime storms in the Sierra Nevada: Sensitivity to the microphysical parameterization and horizontal resolution, *Mon. Weather Rev.*, *133*, 2834–2859, doi:10.1175/MWR3004.1.

Hayes, P. S., L. A. Rasmussen, and H. Conway (2002), Estimating precipitation in the central Cascades of Washington, *J. Hydrometeorol.*, *3*, 335–346, doi:10.1175/1525-7541(2002)003<0335:EPITCC>2.0.CO;2.

Intergovernmental Panel on Climate Change (2007), *Climate Change 2007: The Physical Science Basis. Contribution of Working Group I to the Fourth Assessment Report of the Intergovernmental Panel on Climate Change*, edited by S. Solomon et al., Cambridge Univ. Press, Cambridge, U. K.

Leung, L. R., and Y. Qian (2009), Atmospheric rivers induced heavy precipitation and flooding in the western U.S. simulated by the WRF regional climate model, *Geophys. Res. Lett.*, *36*, L03820, doi:10.1029/2008GL036445.

McNally, A. P., P. D. Watts, J. A. Smith, R. Engelen, G. A. Kelly, J. N. Thèpaut, and M. Matricardi (2006), The assimilation of AIRS radiance data at ECMWF, *Q. J. R. Meteorol. Soc.*, *132*(616), 935–957, doi:10.1256/qj.04.171.

Molotch, N. P. (2009), Reconstructing snow water equivalent in the Rio Grande headwaters using remotely sensed snow cover data and a spatially distributed snowmelt model, *Hydrol. Processes*, *23*, 1076–1089, doi:10.1002/hyp.7206.

Molotch, N. P., and R. C. Bales (2005), Scaling snow observations from the point to the grid-element: Implications for observation network design, *Water Resour. Res.*, *41*, W11421, doi:10.1029/2005WR004229.

Molotch, N. P., and R. C. Bales (2006), SNOTEL representativeness in the Rio Grande headwaters on the basis of physiographics and remotely sensed snow cover persistence, *Hydrol. Processes*, *20*, doi:10.1002/hyp.6128.

Molotch, N. P., and S. A. Margulis (2008), Estimating the distribution of snow water equivalent using remotely sensed snow cover data and a spatially distributed snowmelt model: A multi-resolution, multi-sensor comparison, *Adv. Water Resour.*, *31*, 1503–1514, doi:10.1016/j.advwatres.2008.07.017.

Neiman, P. J., F. M. Ralph, A. B. White, D. E. Kingsmill, and P. O. G. Persson (2002), The statistical relationship between upslope flow and rainfall in California's coastal mountains: Observations during CALJET, *Mon. Weather Rev.*, *130*, 1468–1492, doi:10.1175/1520-0493(2002)130<1468:TSRBUF>2.0.CO;2.

Neiman, P. J., F. M. Ralph, G. A. Wick, J. Lundquist, and M. D. Dettinger (2008a), Meteorological characteristics and overland precipitation impacts of atmospheric rivers affecting the West Coast of North America based on eight years of SSM/I satellite observations, *J. Hydrometeorol.*, *9*, 22–47, doi:10.1175/2007JHM855.1.

Neiman, P. J., F. M. Ralph, G. A. Wick, Y.-H. Kuo, T.-K. Wee, Z. Ma, G. H. Taylor, and M. D. Dettinger (2008b), Diagnosis of an intense atmospheric river impacting the Pacific Northwest: Storm summary and offshore vertical structure observed with COSMIC satellite retrievals, *Mon. Weather Rev.*, *136*, 4398–4420, doi:10.1175/2008MWR2550.1.

Neiman, P. J., A. B. White, F. M. Ralph, D. J. Gottas, and S. I. Gutman (2009), A water vapor flux tool for precipitation forecasting, *Water Manage.*, *162*, 83–94.

Olsen, E. T., E. Fetzer, S.-Y. Lee, E. Manning, J. Blaisdell, and J. Susskind (2007), *AIRS/AMSU/HSB version 5 CalVal status summary*, Jet Propul. Lab., Calif. Inst. of Technol., Pasadena.

Pandey, G. R., D. R. Cayan, and K. P. Georgakakos (1999), Precipitation structure in the Sierra Nevada of California during winter, *J. Geophys. Res.*, *104*, 12,019–12,030, doi:10.1029/1999JD900103.

Ralph, F. M., P. J. Neiman, G. A. Wick, S. I. Gutman, M. D. Dettinger, D. R. Cayan, and A. B. White (2006), Flooding on California's Russian River: The role of atmospheric rivers, *Geophys. Res. Lett.*, *33*, L13801, doi:10.1029/2006GL026689.

Reale, O., W. K. Lau, J. Susskind, E. Brin, E. Liu, L. P. Riishojgaard, M. Fuentes, and R. Rosenberg (2009), AIRS impact on the analysis and forecast track of tropical cyclone Nargis in a global data assimilation and forecasting system, *Geophys. Res. Lett.*, *36*, L06812, doi:10.1029/2008GL037122.

Rutter, N., D. Cline, and L. Li (2008), Evaluation of the NOHRSC snow model (NSM) in a one-dimensional mode, *J. Hydrometeorol.*, *9*, 695–711, doi:10.1175/2008JHM861.1.

Serreze, M. C., M. P. Clark, and A. Frei (2001), Characteristics of large snowfall events in the montane western United States as examined using snowpack telemetry (SNOTEL) data, *Water Resour. Res.*, *37*, 675–688, doi:10.1029/2000WR900307.

Stewart, I. T., D. R. Cayan, and M. D. Dettinger (2004), Changes in snowmelt runoff timing in western North America under a "business as usual" climate change scenario, *Clim. Change*, *62*, 217–232, doi:10.1023/B:CLIM.0000013702.22656.e8.

Tian, B., D. E. Waliser, E. J. Fetzer, B. H. Lambrigtsen, Y. L. Yung, and B. Wang (2006), Vertical moist thermodynamic structure and spatial-temporal evolution of the Madden-Julian oscillation in Atmospheric Infrared Sounder observations, *J. Atmos. Sci.*, *63*, 2462–2485, doi:10.1175/JAS3782.1.

Uppala, S., D. Dee, S. Kobayashi, P. Berrisford, A. Simmons (2008), Towards a climate data assimilation system: Status update of ERA-Interim, *ECMWF Newsl.*, *115*, 12–18.

E. J. Fetzer, B. Guan, and D. E. Waliser, Jet Propulsion Laboratory, California Institute of Technology, 4800 Oak Grove Dr., Pasadena, CA 91109, USA. (bin.guan@jpl.nasa.gov)

N. P. Molotch, Department of Geography, University of Colorado at Boulder, Boulder, CO 80309, USA.

P. J. Neiman, Physical Sciences Division, Earth System Research Laboratory, NOAA, 325 Broadway, Boulder, CO 80305, USA.